



A single-cell atlas reveals the tumorigenesis and microenvironment status of primary tracheobronchial tumors



Chen Shu^{1,2,7}, Xiyang Tang^{1,7}, Kaifu Zheng^{1,3,7}, Runze Zhang^{1,7}, Yulong Zhou¹, Mengchao Li¹, Weiguang Du¹, Yuquan Bai¹, Yang Shen¹, Yujian Liu⁴, Haitang Yang⁵, Feng Yao⁵, Xiaolong Yan¹✉, Nan Ma⁶✉ & Jinbo Zhao¹✉

Primary tracheobronchial tumors (PTBTs) can often be successfully treated by surgery; however, more effective strategies are still warranted for advance tumor cases. The present study aimed to provide a comprehensive understanding of the molecular and cellular features of PTBTs, along with the tumor microenvironment (TME). By performing single-cell RNA, we revealed a distinct TME landscape of PTBTs containing 52,739 single cells. For instance, these three pathological types were found have heterogeneous fibroblast populations, immune cells were more activated in inflammatory myofibroblastic tumor (IMT). Notably, a subpopulation of BIRC5⁺ cells was identified in primary tracheal squamous cell carcinoma (SCC) and adenoid cystic carcinoma (ACC) samples, which may have similar properties to cancer stem cells (CSCs). Moreover, IMT was characterized by the infiltration of pro-inflammatory immune cells, and might be a benign tumor. Importantly, based on ligand-receptor analysis, the PPIA/CD147 pair was found to be strongly upregulated during tumor and CD8⁺ T cell interactions. By applying multiplex immunofluorescence for selected markers, we validated the presence of the separate cell entities. Our findings provide deeper insights into the biology of PTBTs, which may be beneficial for advancing the diagnosis and therapy of PTBTs.

Primary tracheobronchial tumors (PTBTs) are rare lesions that can be benign or malignant. However, regardless of their pathological nature, they can pose a serious threat to the life of patients as they can lead to obstruction of the airways. Cancers of the trachea, bronchus, and lungs represent a huge economic burden worldwide^{1,2}. Of note, squamous cell carcinoma (SCC) and adenoid cystic carcinoma (ACC) account for more than two-thirds of all PTBT cases^{3,4}. Importantly, inflammatory myofibroblastic tumor (IMT) is usually regarded as a benign and interstitial origin airway tumor⁵. PTBTs with size less than 6 cm are commonly treated by surgical resection, but this approach is often ineffective once the tracheal resection length exceeds 50% in adults or 30% in children, as tension-free anastomosis fails, regardless of whether the adjacent tissue has been loosened^{6–8}. Therefore, radiotherapy, chemotherapy, and interventional therapy remain the major methods for

patients with inoperable PTBTs despite their unsatisfactory efficacy^{9,10}. Hence, it is of great value to explore a new succedaneous approach for PTBTs patients with inoperable resection or recurrence.

Nowadays, Immunotherapy is commonly used to specifically target immune checkpoint molecules, such as programmed cell death 1 (PD-1) and programmed cell death ligand 1 (PD-L1)¹¹, and thus enhance the immune response against multiple types of cancer cells, thereby preventing their growth and progression^{12–14}. The basic principle of immunotherapy involves the activation of CD8⁺ T cells and other tumor-killing immune cells, a prerequisite for the clinical immunotherapy implementation^{15,16}. PTBTs were reported to express high levels of PD-L1 in 95% of SCC cells, indicating that these cells may be more sensitive to immunotherapy than other types of PTBTs¹⁷. After investigating the expression of PD-L1 and

¹Department of thoracic surgery, Tangdu Hospital, Fourth Military Medical University, Xi'an, Shaanxi, China. ²Department of Cardiothoracic Surgery, The 902nd Hospital of the Chinese People's Liberation Army Joint Logistic Support Force, Bengbu, Anhui, China. ³Department of General Surgery, The 991st Hospital of the Chinese People's Liberation Army Joint Logistic Support Force, Xiangyang, Hubei, China. ⁴Department of Cardiothoracic Surgery, Central Theater Command General Hospital of Chinese People's Liberation Army, Wuhan, Hubei, China. ⁵Department of Thoracic Surgery, Shanghai Chest Hospital, Shanghai Jiao Tong University, Shanghai, China. ⁶Department of Ophthalmology, Tangdu Hospital, Fourth Military Medical University, Xi'an, Shaanxi, China. ⁷These authors contributed equally: Chen Shu, Xiyang Tang, Kaifu Zheng, Runze Zhang.

✉ e-mail: yanxiaolong@fmmu.edu.cn; manan840808@163.com; zhaojinbo@aliyun.com

CD8⁺ immune cells in 23 patients with PTBTs by immunohistochemical, Tapias et al. concluded that the expression of PD-L1 and the infiltration of CD8⁺ immune cells were higher in SCC rather than ACC, indicating patients with SCC may achieve better treatment results than salivary gland type trachea tumors¹⁸. Likewise, in our previous research, we came to the similar conclusion and found that the immune status of PTBTs is closely related to tumor recurrence¹⁹. Although numerous studies have suggested that immunotherapy may induce long-term PTBTs remission, further studies are still required to unequivocally demonstrate the therapeutic efficacy of immunotherapy for PTBTs^{17,20}. Stromal and immune cells are known to impact the behavior of the TME. Nonetheless, only few studies have explored the features of the TME of PTBTs.

With the advancement of transcriptomic techniques especially the appearance of single-cell RNA-sequencing (scRNA-seq), specific analysis of cell clusters at the single-cell level become truth. In this study, we explored the phenotype of the TME of PTBTs based on scRNA-seq human main trachea or bronchus tissue samples. Overall, we analyzed 52,739 single cells and distinguished 43 cell types, including some that had not been previously identified in the TME of PTBTs to date. Of note, we found endothelial cells (ECs) show upregulated of angiogenesis and downregulated of immune activation in tumor-derived ECs than normal ECs. Furthermore, these three pathological types of PTBTs have heterogeneous fibroblast populations, and immune cells were more activated in IMT. Importantly, we comprehensively explored the different epithelial tumor cells and fibroblasts populations within the TME of different PTBTs types. Based on ligand-receptor analysis and validation analyzes, we found that PPIA/CD147 pair (also known as CypA and BSG) may promote cell proliferation and migration, and induce immune escape in PTBTs, which may explain the relatively poor prognosis of SCC and ACC cases. The data herein collected are expected to pave new foundations for the development of more efficient targeted strategies to tackle PTBTs and enhance the outcome of patients with inoperable tumors.

Results

Clinical resources of patients with PTBTs

We collected clinical data from ten patients of SCC, ACC, or IMT PTBTs, including gender, age, lesion area and so on. All male patients were former smokers and female patients had no history of smoking, while no patients were suffered from chronic obstructive pulmonary disease (Fig. S1A). Next, we exhibited the typical pre- and post-operative chest X ray, chest computed tomography (CT), bronchoscopic photographs from SCC, ACC and IMT (Fig. S1B). Together, these images demonstrate the characteristics of three pathological types of PTBTs.

scRNA-seq atlas of human PTBTs versus normal tissues

Ten patients with untreated SCC, ACC, or IMT underwent surgical resection or bronchoscopic resection. A total of six tumor and normal tissue samples were collected and digested into single-cell suspensions for scRNA-seq analysis (Fig. 1A). In addition, three normal trachea tissues derived from GSE136831 were added for joint analysis. After quality filtering, a total of 52,739 cells were obtained, which were then fit into 34 clusters. Among this dataset, 13,797 (26.2%), 15,912 (30.2%), 17,481 (33.1%), 5549 (10.5%) cells were derived from SCC, ACC, IMT, and normal samples, respectively. t-distributed stochastic neighbor embedding (t-SNE) analysis revealed that the cells were not separated according to their type of tissue of origin (Fig. 1B). Based on marker genes and activated signaling pathways, 10 cell types were identified (Figs. 1B, C, and S2A, B), namely epithelial cells (markers: EPCAM and KRT19), T cells (CD3D and CD3E), natural killer (NK) cells (NKG7 and GNLY), endothelial cells (PECAM1 and PLVAP), B cells (CD79A and MS4A1), fibroblasts (COL1A1 and DCN), myeloid cells (FCGR3A and S100A9), mast cells (MS4A2 and TPSB2), plasma cells (JCHAIN and MZB1), and smooth muscle cells (ACTA2 and MYH11). Although all 10 major cell types were present in both tumor and normal tissues (Fig. 1D), their infiltration grade varied, possibly reflecting the differences between the tissues. As SCC and ACC are predominantly of

epithelial origin, the highest percentage of epithelial cells was found in SCC (73.07%) and ACC (58.42%), while only 34 epithelial cells were found in IMT. Fibroblasts are the most enriched in IMT (32.8%), followed by myeloid cells (30.63%) and T cells (25.6%). In contrast with IMT, myeloid and T cells were less enriched in SCC and ACC, with SCC the least, which indicates that SCC may be the most malignant of these three pathologic types of PTBTs. Furthermore, we identified 43 distinct cell subpopulations, including 5 tumor cell subclusters. Together, these results reveal the differences in the cellular compositions among these three pathologic types tissues.

BIRC5⁺ epithelial cells may contribute for PTBTs progression

Since PTBTs, including SCC- and ACC-derived tumors, are predominantly of epithelial origin, we compared the transcriptional patterns of the SCC- and ACC-derived PTBT cells with those of normal epithelial cells. We re-clustered the epithelial cells within the SCC, ACC, and normal samples, respectively. Unfortunately, only 34 epithelial cells were detected in the IMT samples, which hampered our ability to regroup and analyze them. In agreement with previous reports, we detected basal, club, mucous, and serous cells in the SCC samples (Figs. 2A, and S3A), as well as ionocytes, which are a rare cell type that expresses FOXI1, ASCL3, and CFTR²¹, and are the main source of CFTR activity in the airways (Fig. S3B). Next, analysis of the epithelial cells within the SCC samples using copy number karyotyping of aneuploid tumors (CopyKAT) and differential transcriptional analysis using CytoTRACE^{22,23} revealed six tumor cell clusters and three tumor cell types that were classified as basal tumor, cyclin, and BIRC5⁺ cells (Fig. 2B, C). Basal tumor cells showed a high expression of basal cell-associated markers (TP63 and MIAT), whereas BIRC5⁺ cells were predominantly characterized by high expression of proliferation-related genes (BIRC5, PTTG1, and CENPF) (Fig. S3C). Concerning the ACC samples, the sequential clustering analysis identified myoepithelial, airway submucosal gland (SMG) basal²⁴, basal, ciliated, and tuft cells. In addition, eight tumor cell clusters were identified and classified into three subgroups, namely SMG duct cells²⁴, serous glandular cells, and BIRC5⁺ cells (Figs. 2D, F, and S3D), which were confirmed by immunofluorescence (Fig. 2G). Similarly, we re-clustered the epithelial cells of the normal samples and identified basal, club, ciliated, serous, and mucous cells (Fig. S3E, F). The BIRC5⁺ cell subpopulations identified in all SCC and ACC patient samples showed nearly similar percentages of epithelial cells (6.81% and 7.75%, respectively). Crucially, the key transcriptional programs identified-including the presence of BIRC5⁺ cells-were observed consistently across all SCC and ACC patients, confirming that our findings are not driven by a subset of outliers but represent a common feature of the PTBT microenvironment. Basal tumor cells were the most frequent cell type in the SCC samples (42.09%), followed by basal cells (14.52%). In addition, SMG duct cells accounted for 35.27% of the epithelial cells in ACC samples. These results revealed significant tumor heterogeneity in PTBTs and normal trachea tissues (Fig. S3G). To explore the potential cancerous process of SCC and ACC, we conducted RNA velocity analysis²⁵ and identified that BIRC5⁺ cells were positioned upstream of other tumor cell states (Fig. 2H), suggesting that BIRC5⁺ cells may play a potential progenitor-like role and may have the ability to further differentiate into other tumor cells to maintain the viability of each malignant cell cluster²⁶.

To further analyze the role of BIRC5⁺ cells, gene set variation analysis (GSVA) was performed. GSVA data showed that G2M checkpoint, DNA repair, and E2F targets, which are well-known signaling pathways associated with cell cycle activation, cell proliferation, and invasiveness in multiple cancers²⁷⁻²⁹, were upregulated in epithelial cells of SCC- and ACC-derived PTBTs as compared with normal tissues (Fig. 3A), indicating that BIRC5⁺ cells may have strong self-renewal ability. Moreover, metabolic pathways known to promote tumorigenesis and tumor progression³⁰, such as glycolysis, were found to be upregulated in SCC and ACC tissues. Of note, GSVA analysis revealed distinct transcriptional profiles in all epithelial cells

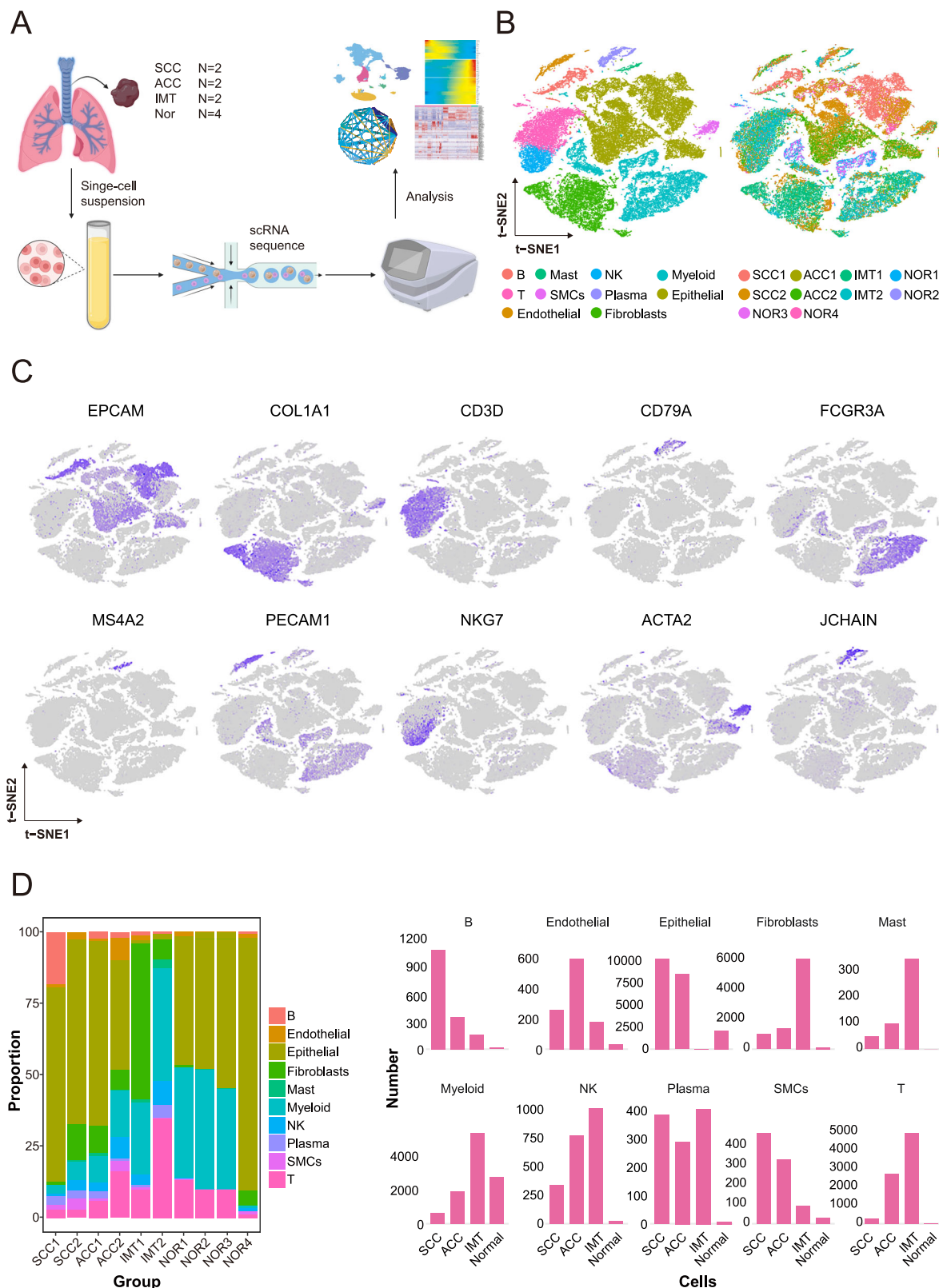


Fig. 1 | Single-cell analysis of primary tracheobronchial tumor and normal trachea samples. **A** Workflow of the sample collection, sequencing and bioinformatic analysis. **B** t-SNE plot of 52,739 cells showing 10 cell types (left) and the sample

origin of the cells (right). **C** Expression of marker genes for the different cell types (defined above each panel). **D** Proportion (left) and number (right) of cells originating from three tumor samples and normal trachea tissue.

between ACC and normal tissues (Fig. S3H). ACC tissues presented persistent activation of one or more highly-conserved signal transduction pathways, such as Notch, Hedgehog, and Wnt beta-catenin pathways, which may help explain the poor prognosis of this type of PTBTs when

treated with chemotherapy and/or radiotherapy³¹. Of note, NOTCH3, which is involved in the Notch signaling, and ASPM, which is involved in the Wnt beta-catenin pathway, were significantly upregulated in ACC samples.

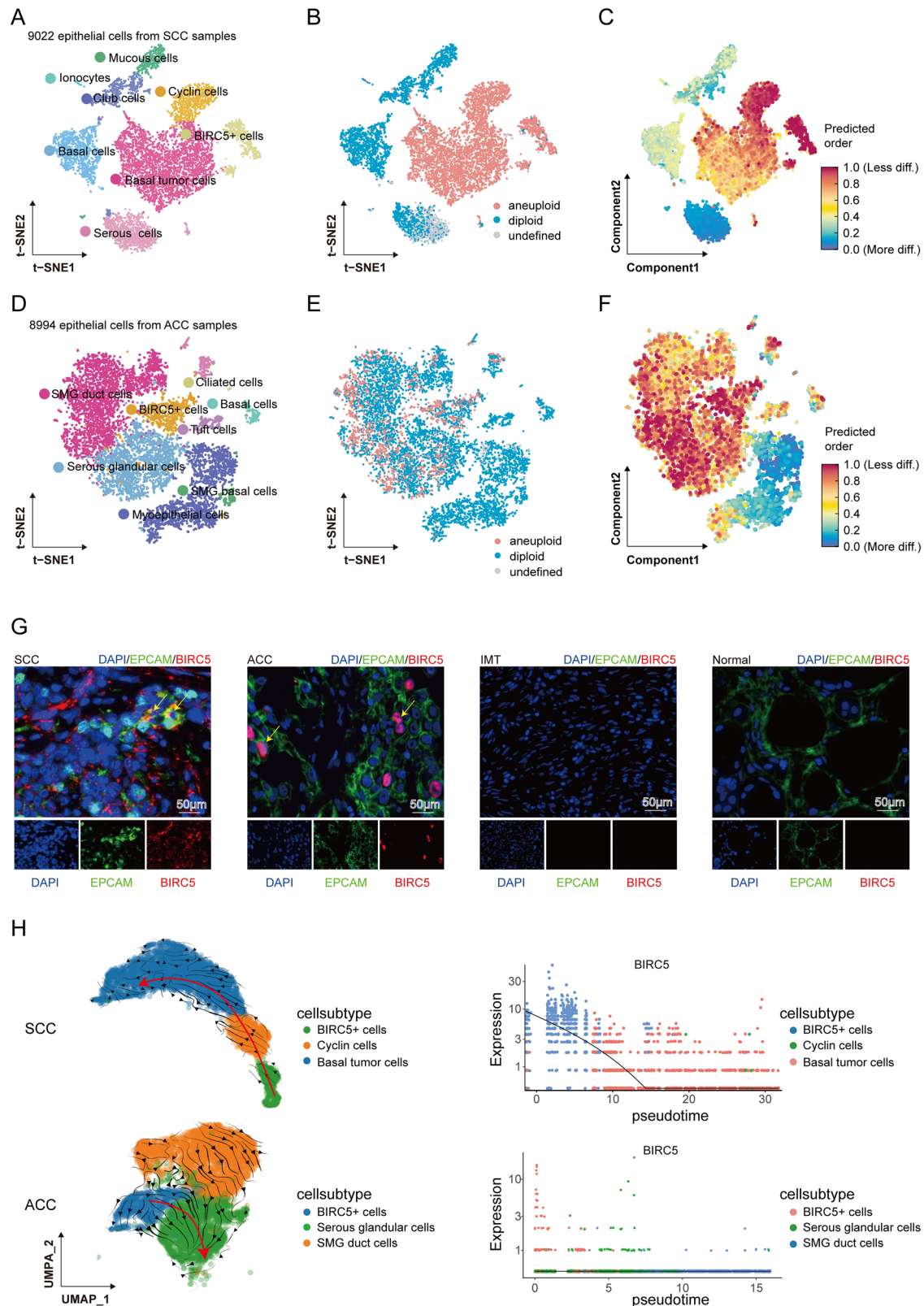
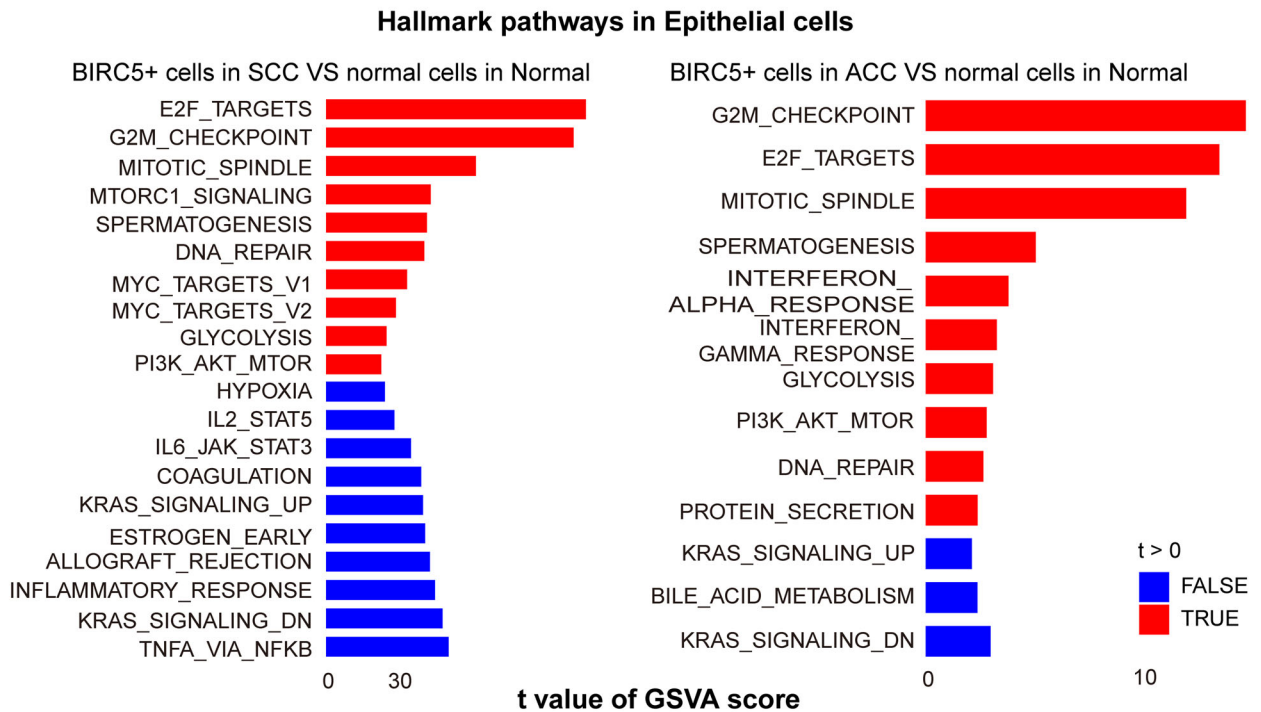


Fig. 2 | Characterization of the epithelial cells in SCC, ACC, and normal tissue samples. **A** t-SNE plots of epithelial cells subgroups within SCC samples. **B** CopyKAT was used to discriminate tumor cells (in red) from normal epithelial cells (in blue) within SCC samples. **C** CytoTRACE results of all epithelial cells representing the degree of differentiation within SCC samples. **D** t-SNE plots of epithelial cells subgroups within ACC samples. **E** CopyKAT was used to discriminate tumor cells (in red) from normal epithelial cells (in blue) within ACC

samples. **F** CytoTRACE results of all epithelial cells representing the degree of differentiation within ACC samples. **G** Immunofluorescence staining showing the expression of key markers BIRC5 and EPCAM in tumor and normal trachea tissues (scale bar, 50 μm). (Yellow arrows indicate representative cells positive for both EPCAM and BIRC5). **H** RNA velocity analysis of the tumor cells and pseudotime expression trends of BIRC5 in SCC and ACC.

A



B

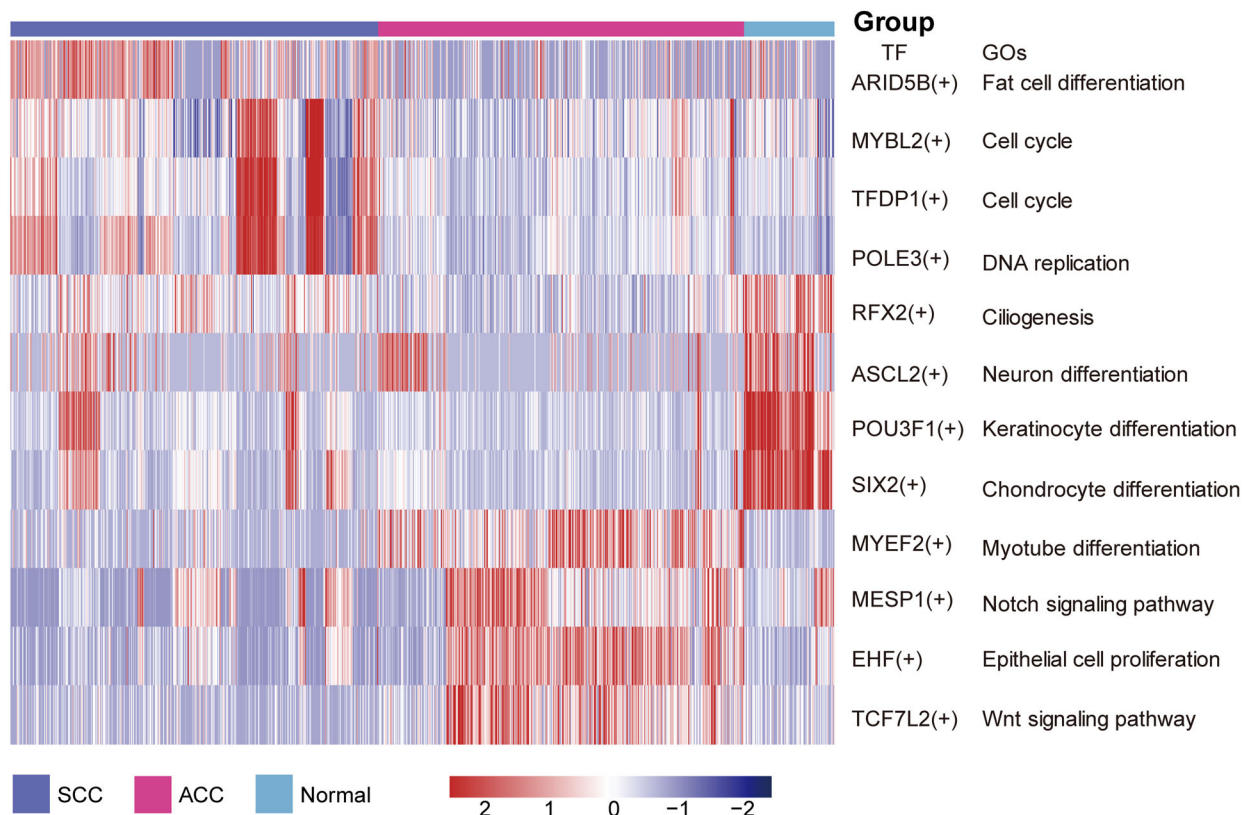


Fig. 3 | Hallmark pathways and transcription factors of epithelial cells in SCC and ACC, compared with normal tissue samples. **A** Comparative analysis of the differently activated signaling pathways activated in BIRC5⁺ cell between tumor (SCC and

ACC) and normal epithelial cells. *t*-values of GSEA scores with a linear model are shown. dn, down; UV, ultraviolet; v1, version 1; v2, version 2. **B** Heatmap of the SCENIC analysis of transcription factors and the downstream gene sets in epithelial cells.

SCENIC analyzes further suggested that MYBL2, which is an essential transcription factor involved in the regulation of various molecular processes in tumorigenesis, including cell survival, proliferation, and differentiation, and is regarded as a poor prognostic

biomarker in multiple cancers³², exhibited high regulatory activity in SCC compared with ACC and normal tissues. In addition, the regulatory activity of MESP1 and TCF7L2, which were reported to be associated with the Notch and Wnt beta-catenin pathways,

respectively, were found to be activated in ACC samples (Fig. 3B), which agreed with the GSVA results.

Fibroblasts may promote proliferation and ECM remodeling of PTBTs

scRNA-seq results allowed to identify 12 fibroblast clusters, among which cluster 0, 2, and 7 were only found in IMT (Fig. 4A). To explore the potential function of these three clusters, we performed Venn diagram and Gene Ontology analysis (Fig. 4B). Extracellular matrix and structure organization features were found to be significantly upregulated in this cell type, and we named it extracellular matrix cancer-associated fibroblasts (eCAFs) (Fig. 4C), which suggest that they may play an essential role in the development of PTBTs by modulating the TME³³. We also identified other six distinct cell types, including five cancer-associated fibroblasts (CAFs) (Fig. S4A), namely SMCs (markers: ACTA2 and RGS5.1), myofibroblastic CAFs (mCAFs) (COL1A1, MMP11, and POSTN), inflammatory CAFs (iCAFs) (CFD, CXCL14, and CXCL12), anti-presenting CAFs (apCAFs) (CD74, HLA-DRA, and HLA-DRB1), and proliferative CAFs (pCAFs) (STMN1, TOP2A, and CENPF) (Fig. S4B, C). Our copy number variation (CNV) analysis further showed that fibroblasts in IMT had low CNV scores compared with T cells and B cells, in line with the results of copyKAT (Figs. 4E, and S4D). Taken together, these results suggest that IMT may be a benign tumor as no tumor cells were found and ECM remodeling may be significantly activated in IMT and accounts for its low-grade but invasive pathological features³⁴ (Fig. S4E).

Next, by using GSVA with respect to the hallmark pathways of cancer, we confirmed our annotations from an orthogonal vantage point³⁵ (Fig. 4F). iCAFs exhibited an upregulation of the IL2-STAT5 pathway, Kras, and complement signaling, which was associated with pro-inflammatory activities. Regarding mCAFs^{36,37}, the upregulated pathways comprised TGF-beta signaling, which is involved in the development of activated myofibroblasts, KRAS signaling, and the pathways underlying the epithelial to mesenchymal transition. The above results support our annotation. Of note, G2M checkpoint, E2F targets, DNA repair and Myc targets were upregulated in this cluster, corroborating the annotation of pCAFs. As previously reported³⁸, MHC-associated genes such as CD74, HLA-DRA, and HLA-DRB1 were highly expressed in apCAFs. GSVA analysis revealed that allograft rejection was the most prominently upregulated signaling pathways among the different fibroblast types.

Tumor endothelial cells can upregulate angiogenesis pathways

When talk to endothelial cells (ECs), 955 cells were found. Re-clustering these 955 ECs revealed 10 clusters (Fig. 5A). All these cells were mixed together, so it was difficult to separate ECs among these three pathologic types tissues and normal tissue (Fig. 5B). All 10 cluster ECs were found in three pathologic types tissues and two normal tissues except cluster 3 (Fig. 5C). According to the marker genes, we identify tumor ECs (HSPG2, cluster 0, 2, 3, 6, 8); blood ECs (FLT1, cluster 0-3, 5, 6, 8); normal ECs (MT2A, cluster 1, 5, 7) and lymphatic ECs (PROX1, cluster 4) (Fig. 5D).

We next performed analysis of hallmark pathway gene signatures. GSVA results showed that MYC Targets V1, Notch signaling pathway, and angiogenesis in tumor ECs were upregulated compared with normal ECs, while MYC Targets V1 was reported to be important for tumor angiogenesis³⁹ (Figs. 5E, and S4E). Also, Notch signaling pathway is regarded as to play a crucial role in angiogenesis and tumorigenesis of non-small cell lung cancer through NOTCH1⁴⁰. Other pathway related to angiogenesis, such as hypoxia pathway was also upregulated, indicating that angiogenesis was higher in tumor ECs than normal ECs. Furthermore, E2F targets, G2M checkpoint and DNA repair were significantly upregulated, indicating that tumor ECs may promote tumor progression.

We demonstrated that gene related to angiogenesis, such as NOTCH1 was found high expression in tumor ECs, as was the

expression of MMP2, ANOPT2, HSPG2, HIFA and CCN2 (Fig. 5F). Furthermore, the genes involved in immune activation and chemotaxis (CCL5, CXCL11) were downregulated. In brief, this indicated that tumor ECs may downregulate their immune activation ability, which can induce tumor escape.

Finally, we employed SCENIC analysis to assess the regulation activity of expression differences in transcription factors between tumor ECs and normal ECs. The SCENIC results suggested that SOX4, ELK3, MEF2A, NFE2L1, and KLF2 were high regulatory activity transcription factors, while ZNF76, RFX5, BRF1, THAP11, and ZNF274 were low regulatory activity transcription factors (Fig. 5G). SOX4 was considered to play an important role in immune evasion in tumor cells⁴¹. Likewise, ELK3 was reported to regulate cell migration and may facilitate tumor metastasis⁴². The transcription factors RFX5 can strengthen the expression of HLA-DR molecules and binds to all MHC inducers, which can promote immune activation^{43,44}. Together, we found that tumor ECs can upregulate angiogenesis pathway and downregulate immune activation pathway.

Tumor T cells in SCC showed higher immune-suppressive status compared with ACC and IMT

T cells were an essential component and the most common immune cell type of TME in PTBTs. In this study, we identified 7 cell types according to the marker genes (Fig. 6A, B). Among these T cell types, stress response state CD8⁺ T cells (Tstr), effector CD8⁺ T cells (Tef), CD4⁺ T helper cells (Th), regulatory T cells (Tregs), exhausted T cells (Tex), IFN response associated T cells (Tisg) and natural killer cells (NK) were identified (Fig. 6C). Tstr cells was regarded as a new cell type which reflected cell stress response state and may be associated with immunotherapy resistance in nonresponsive tumors⁴⁵. Some research also revealed that Tstr cells may play an essential role in tumor promoting in acute inflammation environment⁴⁶. In this study, CD8⁺ Tstr cells was the most enriched cells, and CD8⁺ Tef cells appeared the least enriched in SCC, compared with ACC and IMT, which indicated CD8⁺ T cells appeared lower cytotoxic activities and stronger tumorigenesis in SCC (Fig. 6D). Of note, CD4⁺ Th cells were found most enriched in IMT compared with SCC and ACC. In our study, CD4⁺ Th cells were mainly characterized by high expression of CD40LG, which usually interacted with CD40 to trigger immune overactivation of immune cells leads to an overproduction of immune response cascades and enhance a powerful tumor-specific T-cell immunity⁴⁷.

We next performed the GSVA analysis to compare the differences of T cells among these three PTBTs pathological types. In CD8⁺ T cells, metabolism pathways such as glycolysis, myogenesis and fatty acid metabolism were upregulated in SCC, suggesting a stronger transcriptional activation status (Figs. 6E, and S5A). However, interferon response, complement and oxidative phosphorylation were significantly upregulated in IMT, indicating a higher inflammatory response activation. When it comes to ACC, Notch signaling and Wnt beta-catenin signaling pathway were found upregulated. Notch signaling pathway has been shown to attenuate the activation of CD8⁺ T cells in lung adenocarcinoma and colorectal carcinoma^{48,49}. Also, the activation of Wnt beta-catenin signaling pathway may decrease T cell infiltration into the TME and induce tumor immune escape⁵⁰.

CD4⁺ T cells are regarded to play an essential role in immunosurveillance and immunotherapy response of tumors. Our GSVA analysis results showed that glycolysis and fatty acid metabolism were upregulated in SCC, which also suggesting a stronger transcriptional activation status, so as NK cells (Fig. 6F, and S5B). In line with CD8⁺ T cells, Notch signaling, Wnt beta-catenin signaling pathway were found upregulated in ACC, compared with SCC and IMT. IMT were characterized by the higher activation of allograft rejection, complement and inflammation response, which consisted with the pathological features of high immune cell infiltration⁵¹.

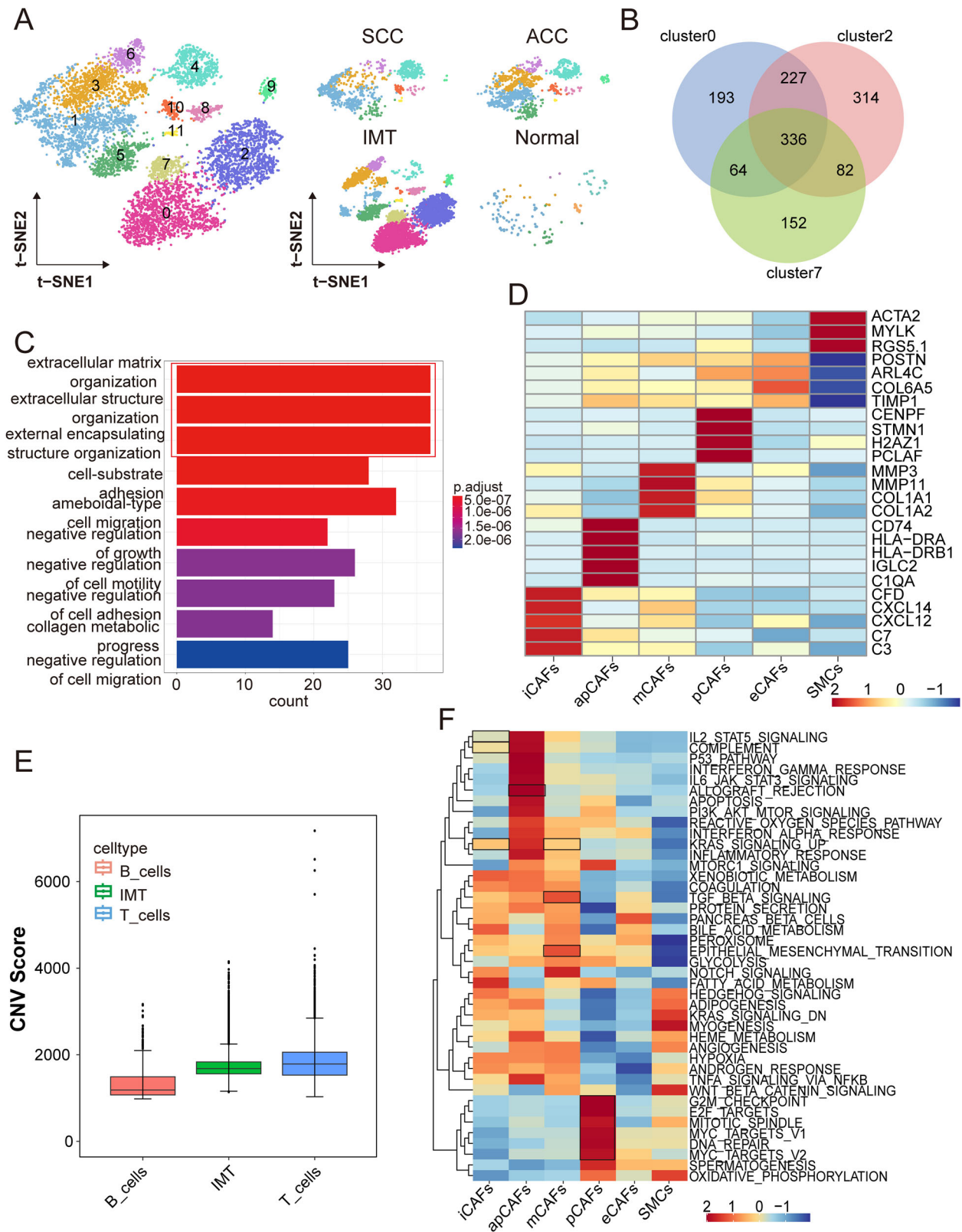


Fig. 4 | Characterization of the fibroblast populations in SCC, ACC, and normal tissue samples. A t-SNE plot of fibroblasts revealing 12 clusters and the sample differences. B Venn diagrams illustrating the overlap of differentially-expressed genes shared among the 3 clusters (cluster 0, 2, and 7) from eCAFs. C Kyoto Encyclopedia of Genes and Genomes (KEGG) analysis showing the main activated

pathways of eCAFs. D Heatmap showing the expression of marker genes of different fibroblast subpopulations. (Red presents high expression and blue presents low expression). E InferCNV score of fibroblasts from IMT compared with T cells and B cells. F GSEA of the hallmark pathways in different fibroblast subpopulations.

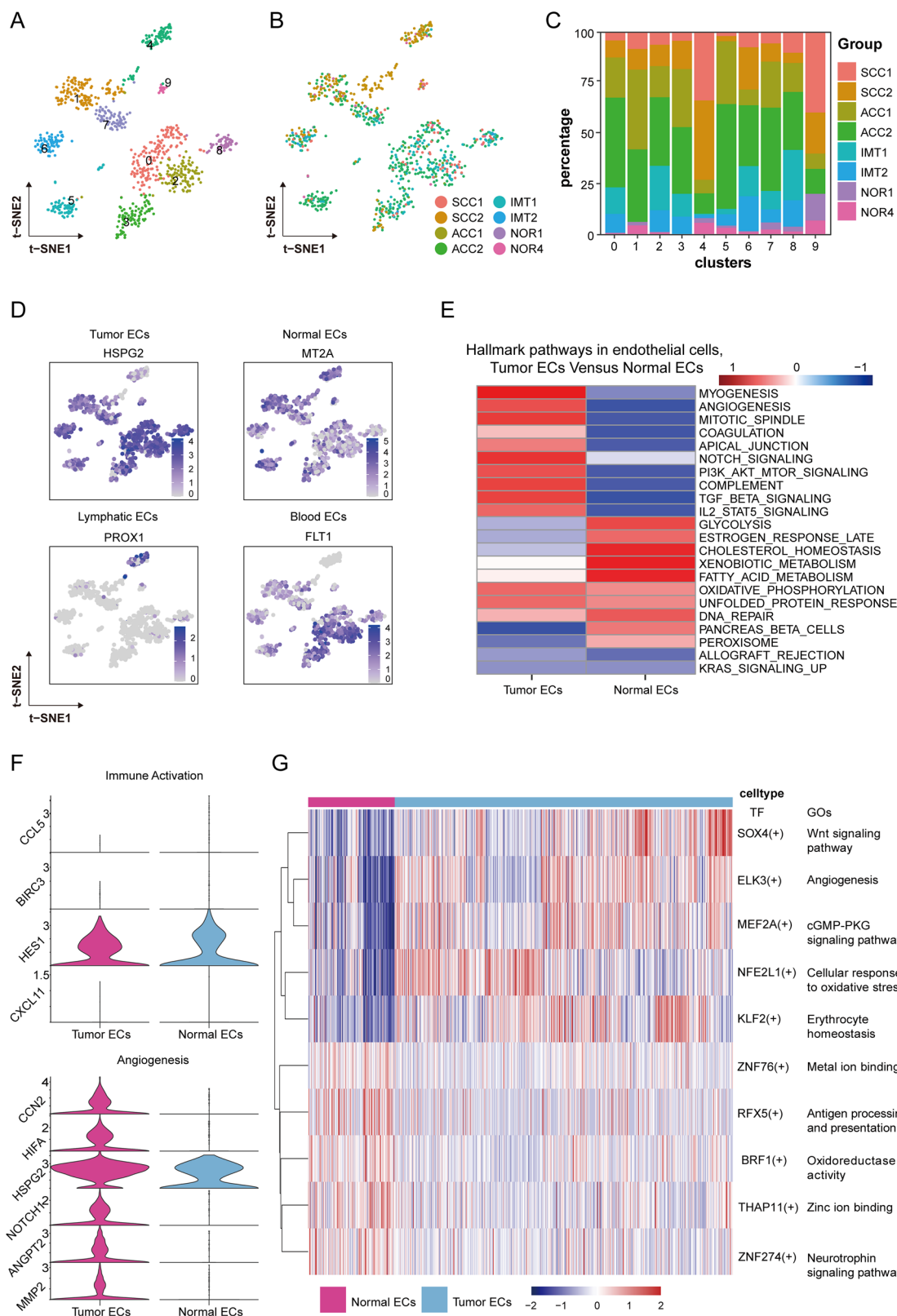


Fig. 5 | Endothelial cells clusters. **A** t-SNE plotting of ECs revealing nine clusters; **B**, **C** The sample origin of ECs; **D** Expression of marker genes identified the ECs as Tumor ECs, Normal ECs, Lymphatic ECs and Blood ECs; **E** Heatmap of GSVA analysis of the hallmark pathways in ECs between Tumor ECs and Normal ECs;

F The key genes expression of immune activation and angiogenesis in Tumor ECs and Normal ECs; **G** Heatmap of the SCENIC analysis of transcription factors and the downstream gene sets in Tumor ECs and Normal ECs.

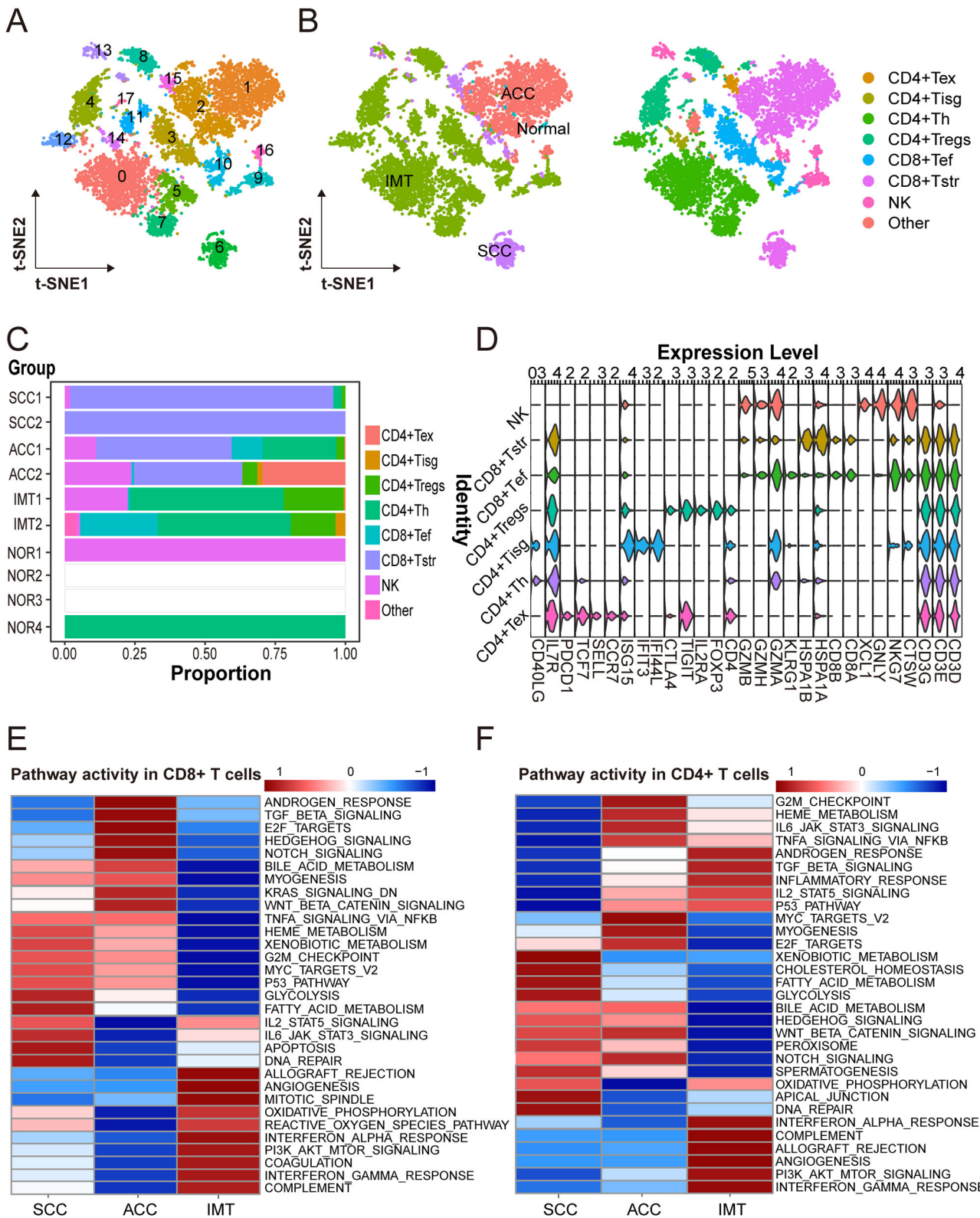


Fig. 6 | T and NK cells clusters. **A** t-SNE plotting of T and NK cells revealing 11 clusters and identified seven T and one NK cell subtypes; **B** The sample origin of T and NK cells; **C** The fraction of T and NK cells originating from three tumor samples and normal trachea tissue. **D** Violin plots showing the expression distribution of

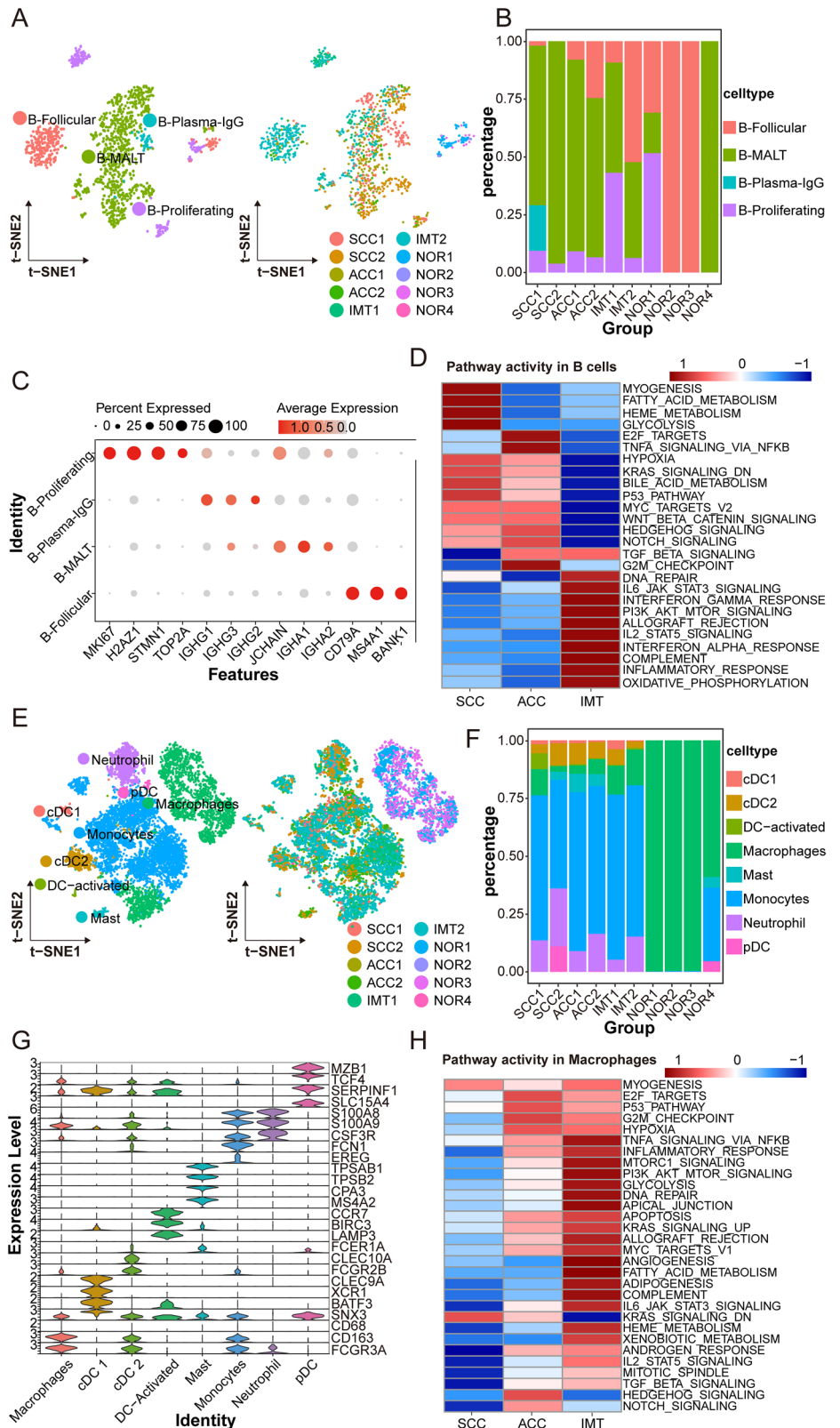
selected special marker genes of T and NK cell subtypes. **E** Heatmap of GSVA analysis of the hallmark pathways in CD8⁺ cells among SCC, ACC and IMT; **F** Heatmap of GSVA analysis of the hallmark pathways in CD4⁺ cells among SCC, ACC and IMT.

B cells were the most enriched in IMT

B cells were considered as an important component of TME. We detected 1103 B cells and revealed 8 clusters. Based on the marker genes, we identified Follicular B cells (B-Follicular, cluster 1; MS4A1), plasma B cells expressing

immunoglobulin gamma (B-Plasma-IgG, clusters 0 and 2; IGHG1), mucosa-associated lymphoid tissue-derived (MALT) B cells (B-MALT, cluster 3 and 4), and proliferating B cells (B-Proliferating, cluster 7; TOP2A) (Fig. 7A). The percentage of B-MALT were the lowest and B-Follicular were

Fig. 7 | B and Myeloid cells clusters. **A** t-SNE plotting of B cells revealing eight clusters and identified four cell subtypes; **B** The fraction of B cells originating from SCC, ACC and IMT; **C** Dot plots showing the expression distribution of selected special marker genes of B cell subtypes; **D** Heatmap of GSVA analysis of the hallmark pathways in B cells among SCC, ACC and IMT; **E** t-SNE plotting of Myeloid cells revealing 15 clusters and identified eight cell subtypes; **F** The fraction of Myeloid cells originating from three tumor samples and normal trachea tissue; **G** Violin plots showing the expression distribution of selected special marker genes of Myeloid cell subtypes; **H** Heatmap of GSVA analysis of the hallmark pathways in macrophages among SCC, ACC and IMT.



found the most enriched in IMT, compared with ACC and SCC. There was no significant difference in the proportion of B-Plasma-IgG among the three pathological types (Fig. 7B). Besides, B-Proliferating expressed high levels of proliferating-associated markers, such as MKI67, TOP2A and STMN1 (Fig. 7C).

The results of GSVA analysis revealed that the immune response was the most upregulated in IMT, compared with ACC and SCC (Figs. 7D, and S6A). In addition, complement and interferon response also significantly upregulated in IMT, suggesting immune cells were activated to promote inflammation response³².

Macrophages tend to become proinflammatory phenotype and promote angiogenesis in IMT

The proportion of myeloid cells was found the highest in IMT than other pathologic types tissues and normal tissue (Fig. 1D). We next regrouped 7507 myeloid cells and revealed 15 clusters (Fig. 7E). One cluster corresponded to neutrophil (cluster 11, S100A9), and six cluster to dendritic cells (DC): activated DC (DC-activated, cluster 14, FCN1), plasmacytoid DC (pDC, cluster 13), conventional DC1 (cDC1, cluster 12), and conventional DC2 (cDC2, cluster 5, 6 and 9). We also identified mast cells with high expression of TPSB2 (cluster 7) and monocytes (cluster 2), while remain six clusters were identified as macrophages (cluster 0, 1, 3, 4, 9 and 10). Of note, macrophages were mainly derived from ACC (52.81%) and IMT (54.89%), compared with SCC (39.08%), suggesting that a stronger activation of innate immune system (Fig. 7F, G).

To dissect the activation of hallmark pathways, we performed GSEA analysis in macrophages. In line with B cells, immune response was significantly upregulated in IMT, compared with SCC and ACC, indicating an inflammation state in which macrophages were infiltrated (Fig. 7H, and S6B). Of note, mTOR1⁵³, Notch⁵⁴ and NF- κ B⁵⁵ signaling were activated, indicating that macrophages in IMT more likely turned into proinflammatory macrophages. Macrophages were reported to can promote metastasis and angiogenesis in TME⁵⁶. In this study, TGF β 1 and angiogenesis pathways were upregulated, suggesting macrophages in IMT may promote angiogenesis.

BIRC5⁺ cells and CD8⁺ T cells may mediate PTBTs immune response

Intercellular communication facilitated by ligand-receptor compounds is crucial for orchestrating a wide range of biological functions, including development, differentiation and inflammation. Therefore, cell-cell interactions between BIRC5⁺ cells and T cells were evaluated using CellphoneDB, a new repository of ligands, receptors, and their interactions that can allow the study of how context-dependent crosstalk between different cell types enables physiological processes to occur⁵⁷. Overall, BIRC5⁺ cells showed strongest interaction with CD8⁺Tstr cells, followed by NK cells, and then CD8⁺Tef and CD4⁺T cells (Fig. 8A). Furthermore, several receptor-ligand pairs between BIRC5⁺ cells and CD8⁺Tstr and CD8⁺Tef cells were identified. Among these, CD147/PPIA (also known as BSG and CYPA, respectively) interaction was found upregulated (Fig. 8B); thus, PPIA may play an essential role in PTBTs immunoregulation via CD147/PPIA, which was validated by multiplex immunofluorescence. At the same time, it was observed that BIRC5 co-localized with CD8 on the surface of tumor cells, further illustrating the molecular interaction between BIRC5 and CD8 (Fig. 8C). Of note, CD147/PPIA interaction was previously identified as a potential therapeutic target for cancer, with CD147 being associated with cancer progression, overall survival, and prognosis of different cancer types, especially at early cancer stages^{58,59}. Moreover, CD147 is highly expressed in cancer and CD8⁺T cells, and can regulate antitumor CD8⁺T cell responses to promote tumor immune escape⁶⁰. Through the interaction with CD147, PPIA overexpression facilitates the proliferation, migration, therapeutic resistance, and stem cell-like properties of cancer cells, so as in our study (Fig. 8D), and is associated with a poor prognosis in cancer patients^{61,62}. In our study, we overexpressed PPIA in two tracheal epithelial cell lines (HBE and BEAS-2B cells (human bronchial epithelial cells) and found that it promoted cell proliferation and migration capabilities (Fig. S7A–E). Alternatively, by co-culturing PPIA-overexpressing BEAS-2B cells with Jurkat T cells and human peripheral blood cells, we found that PPIA could promote the apoptosis of T cells (Fig. S8A–D). In summary, CD147/PPIA interactions may play a crucial role in cell proliferation, migration, and immunoregulation in PTBTs. In addition, we found that BIRC5⁺ cells may also interact with CD8⁺T cells through CD58/CD2 axis, which was considered to be associated with immune evasion in melanoma tumors⁶³. Together, BIRC5⁺ cells and CD8⁺T cells may mediate PTBTs immune response.

Discussion

In this study, we reveal the characteristics of PTBTs and their micro-environmental status at the single-cell level for the first time. Our results confirm many essential conclusions achieved at the histological level and further explore the mechanism of tumor development and biological behavior of PTBTs. By identifying new cell populations and clarifying pathway activation, we gain a more comprehensive understanding of the underlying molecular differences among the PTBTs pathological types, as well as of their specific TME, which may act as a reference book to promote the advancement of PTBTs.

The activity and differentiation of tumor cells are related to the biological properties of tumors. In our study, for the first time, we revealed the different activation of signaling pathways of three pathological types of PTBTs at the single-cell level. However, we found that they may be derived from progenitor cells of the same origin. We demonstrated that SCC and ACC, as tumors of epithelial origin, have different cellular pathways activated during tumorigenesis and development, whereas IMT, a tumor of fibroblast origin, is a benign tumor in which the fibroblasts undergo proliferation but lack tumor differentiation characteristics. Of note, while it is traditionally speculated that SCC and ACC may originate from basal cells and glandular ductal epithelial cells of tracheobronchial origin, respectively, our study revealed that these two PTBTs may have the same potential, functioning as progenitor-like cells, BIRC5⁺ cells, and by using RNA velocity and CytoTRACE analysis, we confirmed that BIRC5⁺ cells are at the initial stage of differentiation in both epithelial-derived tumors. We further confirmed that BIRC5⁺ cells were expressed in both SCC and ACC, but not found in IMT and normal tracheal epithelium by double-labeling immunofluorescence. More importantly, the ligand-receptor analysis showed that BIRC5⁺ cells were able to induce an immune-tolerant microenvironment via CD147/PPIA and CD58/CD2, which may play an important role in tumor development. Our study suggests that BIRC5⁺ cells may play a potential progenitor-like role in both SCC and ACC, and may be an important target for drug therapy intervention.

The TME, which is composed of various cell types, is known to be inextricably linked to cancer cells, serving as a sophisticated ecosystem that supports tumor growth and metastatic dissemination, while attenuating immunological surveillance^{64,65}. Interactions between stromal and tumor cells within the TME can significantly affect tumor progression, as well as antitumor immune responses and therapeutic effects^{66–68}. Herein, we distinguished 38 stromal cell types within the PTBTs microenvironment by specific marker genes and the activation of signaling pathways, indicating that they depicted as separate biologic entities. Our sequencing results revealed that SCC, ACC, and normal tracheal tissues have a higher proportion of epithelial cells than IMT cases. In contrast, the TME of IMT principally consisted of fibroblasts, myeloid cells, and T cells, which aligns with the finding of previous reports that suggested that IMT have a mesenchymal tissue origin that is accompanied by inflammatory infiltration of plasma cells and lymphocytes⁶⁹. Goveia et al. revealed that the heterogeneity of tumor ECs was associated with the poor prognosis of non-small cell lung carcinoma patients, suggesting active angiogenesis may promote tumorigenesis⁷⁰. Our sequencing results showed that tumor ECs expressed higher upregulation of angiogenesis and angiogenesis associated pathways and lower levels of immune activation than normal ECs, indicating ECs may play an essential role in tumor growth by promoting angiogenesis and inhibiting anti-tumor immunity. Importantly, regarding fibroblasts, we found that iCAFs were present in SCC and ACC in high proportions, whereas eCAFs were only present in IMT. These findings suggest that ECM remodeling may be significantly activated in IMT, which accounts for the low-grade but invasive pathological features of this type of PTBTs³⁴.

Immune cells may both play anti-tumor and pro-tumor roles due to their different phenotypes during the process of tumor development. CD8⁺T cells were found more enriched in SCC compared with ACC, which was consistent with previous reports^{18,19}. However, the majority of CD8⁺T cells expressed cell stress response state and may induce an immune-suppressive status that promote tumorigenesis. When it comes to myeloid cells and B

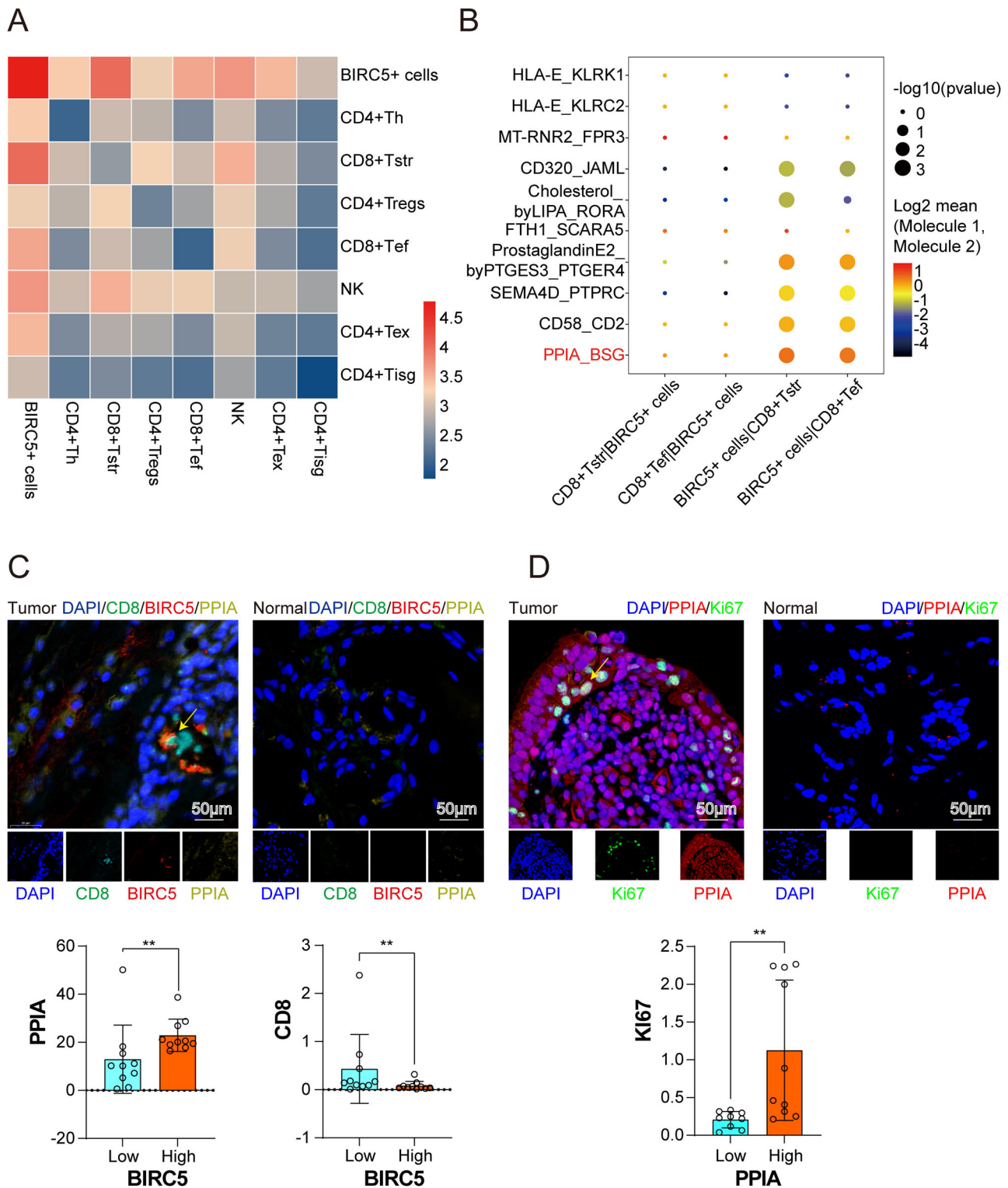


Fig. 8 | BIRC5⁺ cells and CD8⁺ T cells may mediate PTBTs immune response. **A** Heatmap of the degree of potential ligand-receptor pairs between BIRC5⁺ cells and T cells determined by CellphoneDB analysis. **B** Bubble plots showing the 10 main ligand-receptor pairs between BIRC5⁺ cells and CD8⁺ T cells. **C** Multiple immunofluorescence staining of BIRC5⁺ cells for PPIA and CD8 markers in tumor

and normal trachea tissues (scale bar, 50 μ m). Quantitative results of CD8 and PPIA in the high and low expression groups of BIRC5. **D** Immunofluorescence staining of Ki67 in PPIA⁺ cells in tumor and normal trachea tissues (scale bar, 50 μ m). Quantitative results of Ki67 in the high and low expression groups of PPIA.

cells, B cells and macrophages were more enriched in IMT and expressed a higher inflammation state compared with SCC and ACC. Furthermore, macrophages were more likely turned into pro-inflammatory macrophages and may promote angiogenesis in IMT. Our results revealed that these cells were actively involved in tumor progression.

PTBTs remain an unfamiliar clinical area for many thoracic surgeons because of their low morbidity rates. To date, no consensus guidelines have been established for managing PTBTs, and surgery is the most effective treatment for patients with operable indications⁷¹. Accumulating evidence suggests that the tumor microenvironment in SCC exhibits a higher degree

of immune cell infiltration and elevated PD-L1 expression, which may underlie its superior responsiveness to immunotherapy compared to ACC^{18,19}. In contrast, ACC is characterized by invasive growth with a high propensity for submucosal and perineural spread, frequently resulting in positive margins after surgery^{72–74}. Consequently, the standard management of ACC typically involves extended resection combined with adjuvant radiotherapy to improve clinical outcomes. For IMT, which are relatively radioresistant and largely unresponsive to immunotherapy, extended surgical resection constitutes the cornerstone of therapy. Our single-cell data revealed a shared potential progenitor-like cell population between SCC and ACC, suggesting its potential as a novel therapeutic target for immunotherapy. Furthermore, activation of the Notch and Wnt beta-catenin pathway imply a potential therapeutic benefit from targeted inhibitors, which may lead to more effective treatment strategies for ACC patients.

There were also some limitations in our research. First of all, the sample sizes are limited because the relative low morbidity of PTBTs, which may make our data less convincing. It should be noted that the heterogeneity observed across the samples, especially the notable heterogeneity in SCC, could render our results less universally applicable. Due to limited cell availability, T cells, B cells, and fibroblasts isolated from normal samples could not be sufficiently procured for downstream analyzes. Furthermore, due to the lack of mature primary tumor cell lines, the validation portion of our experiments could not be carried out successfully, which greatly limited our therapeutic translations. More importantly, functions of BIRC5⁺ cells could not be investigated individually as they could not be sorted and characterized using flow cytometry. Last but not the least, our study lacks spatial transcriptomic data, which limits in-depth analysis of the spatial distribution relationships of cells within the tumor microenvironment. In the future, we will conduct research with larger sample sizes and integrate multi-omics technologies.

In summary, this study provides a comprehensive overview of the molecular and cellular basis of the different pathological types of PTBTs and highlights the cellular heterogeneity of these rare cancers. Comprehending the state of the TME, as well as the properties and function of cancer cells, is critical to developing new strategies for tumor therapy.

Methods

Human tracheobronchial samples collection, tissue dissociation and preparation of single cell suspensions

After obtaining the consent of the patient or their guardian, approval from the local medical ethics code (No. 202112-05) of Tangdu Hospital of the Fourth Military Medical University and conducted in accordance with the declaration of Helsinki, tumor tissues of patients with PTBTs were preserved in specific tissue preservation solutions and transferred to the laboratory for tissue shredding and digestion with enzymes. Tissues were dissociated into single cells using a dissociation solution composed of 0.35% collagenase IV, 2 mg/mL papain, and 120 Units/mL DNase I, in a 37 °C water bath with shaking at 100 rpm for 20 min. The enzymatic digestion was halted by adding 1× PBS containing 10% fetal bovine serum (FBS, V/V), followed by gentle pipetting 5–10 times with a Pasteur pipette to ensure thorough mixing. The resulting cell suspension was then filtered through a 70-µm to 30-µm stacked cell strainer and centrifuged at 300 × g for 5 min at 4 °C. The cell pellet was subsequently resuspended in 100 µL of 1× PBS (0.04% BSA) and treated with 1 mL of 1× red blood cell lysis buffer (MACS 130-094-183, 10×), incubating at room temperature or on ice for 2–10 min to lyse any remaining red blood cells. After incubation, the suspension was centrifuged again at 300 × g for 5 min at room temperature. The supernatant was carefully aspirated, and the cells were resuspended in 100 µL of Dead Cell Removal MicroBeads (MACS 130-090-101). Dead cells were removed using the Miltenyi® Dead Cell Removal Kit (MACS 130-090-101). The suspension was then resuspended in 1× PBS (0.04% BSA) and centrifuged at 300 × g for 3 min at 4 °C, a step repeated twice to ensure cell purity. Finally, the cell pellet was resuspended in 50 µL of 1× PBS (0.04% BSA). Cell viability was assessed using the trypan blue exclusion method, with the desired viability being above 85%. Single cell suspensions were counted using a

hemocytometer or a Countess II Automated Cell Counter, and the concentration was adjusted to a range of 800–1400 cells/µL. This research was approved by the Ethics Committee of the Fourth Military Medical University (No. 202112-05).

scRNA-seq and bioinformatics analysis

10× Genomics Chromium Single-Cell Kit (V3), in accordance with the specifications of manufacturer, along with a 10× Chromium system (Single Cell Discoveries) was adopted to analyze these ten tissues from GSE136831 (001C; 002C; 003C) and our scRNA-seq data. Next, cDNA amplification and library construction were utilized on the basis of the standardized protocols. Libraries were sequenced by LC-Bio Technology and Seurat (version 4.1.0) was used to select samples that passed quality control and datasets with at least 500 cells. Other filters included quality filtering and double removal methods. Uniform Manifold Approximation and Projection and t-SNE were employed to visualize and explore the sequencing datasets. CopyKAT and CNV analysis were performed to distinguish tumor cells from normal cells in each sample. CytoTRACE and RNA velocity analysis was employed to identify the differentiation state of each cell. GSVA were performed using OmicStudio tools (<https://www.omicstudio.cn/tool>) to extrapolate the level of activation of the gene sets/pathways. SCENIC analysis was used to assess transcription factor expression in different types of PTBTs (SCENIC version 0.11.2). CellphoneDB (<https://www.cellphonedb.org/>) was used to predict abundant ligand-receptor interactions and expression of them between two cell types.

Immunofluorescence staining

Cells were evenly seeded on the center of a glass slide at a density of ~70% and were then incubated for 20 min at room temperature with 100 µL of membrane-breaking solution (Servicebio). The slides were washed three times with phosphate-buffered saline solution and then incubated with anti-BIRC5, anti-CD8, anti-EPCAM, anti-Ki67 and anti-PPIA polyclonal antibodies (1:100 dilution; all from Proteintech) at 4 °C overnight. The slides washed again three times and incubated with the respective secondary antibody for 50 min at room temperature. The cell nuclei were stained with 4',6-diamidino-2-phenylindole before sealing with antifade mounting solution.

Cell culture and PPIA overexpression

HBE and BEAS-2B cells (human bronchial epithelial cells; Procell) were cultured in RPMI 1640 medium (Gibco) with 10% FBS at 37 °C in 5% CO₂. Jurkat cells (human T lymphocyte cells; iCell Bioscience) were cultured in RPMI 1640 medium with 12% FBS at 37 °C in 5% CO₂. PBMCs were collected from health donors.

Cell coculture

Direct coculture was performed in 10 cm plates. Briefly, BEAS-2B (1 × 10⁶ cells) were seeded and cultured in RPMI 1640 medium supplemented with 10% FBS for 24 h. Jurkat and PBMCs (1 × 10⁶ cells each) were directly mixed with BEAS-2B and cultured in RPMI 1640 medium (3 mL) supplemented with 12% FBS for 36 h. Jurkat T cells and PBMC were collected for apoptosis analysis.

Western blot

A total protein collection kit (Invent Biotechnologies) was used to collect total protein. The cells were lysed on ice with SD-001 buffer for 15 min and the lysate was centrifuged at 12,000 rpm for 30 s. An appropriate 5× protein loading buffer was added and the samples were boiled for 10 min. The amount of extracted protein was estimated using a bovine serum albumin assay kit (Beyotime). Based on the collected protein concentration, an appropriate amount was separated by electrophoresis on a 10% sodium dodecyl sulfate-polyacrylamide gel at 300 mA for 60 min. The proteins in the gel were then transferred to nitrocellulose membranes, blocked using QuickBlock (Beyotime) at room temperature, and incubated overnight at 4 °C using anti-FGL1 polyclonal antibody (1:250 dilution; Proteintech). The

membranes were then incubated with a secondary antibody for 60 min at room temperature, washed three times with Tris-buffered saline containing Tween 20, and incubated in a chemiluminescent horseradish peroxidase substrate (Millipore) for 1 min for detection using a visualizer (Tanon).

Cell Counting Kit 8

All cells were collected and resuspended in 1 mL of RPMI 1640 medium (Gibco), and cell density was measured using an electronic cell counter (Olympus). Then, 1000 cells were counted and seeded in 96-well plates (Agilent) in 200 μ L of RPMI 1640 medium. Cell viability was measured using a Cell Counting Kit 8 kit (NCM Biotech) and cell density values were measured at 490 nm for five consecutive days.

Colony formation

HBE and BEAS-2B cells were collected and seeded in 6-well plates (Agilent) at a density of 1000 cells per well in 2 mL of RPMI 1640 medium. After 1 week of culture, the plates were washed three times with phosphate-buffered saline and the cells were fixed with methanol for 20 min. Lastly, the cells were stained with crystal violet for 30 min and photographed.

Scratch assay

Transfected cells were seeded into culture plates and a gap in the cell layer was created using a pipette tip. The culture plates were photographed and wound widths were recorded at 0, 24, and 48 h.

Transwell assay

All cells were collected and resuspended in 1 mL of RPMI 1640 medium (Gibco), and cell density was measured using an electronic cell counter (Olympus). Then, 3×10^4 BEAS-2B cells and 7×10^4 HBE cells were seeded in the top chamber of a Transwell (Costar) and cultured for 24 and 36 h, respectively. Invading cells were stained and counted. Each experiment was repeated three times.

Statistical analysis

Prism 9.0.0 (GraphPad Software) and SPSS 26 (IBM Corp.) were used to perform the statistical analyzes. All data are presented as mean \pm standard deviation. Differences between two groups were assessed by unpaired Student's *t* tests or Wilcoxon test. *p*-value < 0.05 was considered statistically significant.

Data availability

The scRNA sequencing datasets generated in this study can be found in the data depository GEO dataset as GSE 293360.

Code availability

All original code has been uploaded as Supplementary information and is publicly available as of the date of publication. The software versions used and the specific variables or parameters employed for generating or analyzing the current dataset can be found in the corresponding methods section.

Received: 11 June 2025; Accepted: 17 November 2025;

Published online: 13 December 2025

References

- Chen, S. et al. Estimates and projections of the global economic cost of 29 cancers in 204 countries and territories from 2020 to 2050. *JAMA Oncol.* **9**, 465–472 (2023).
- Liu, Y. et al. Disease burden and prediction analysis of tracheal, bronchus, and lung cancer attributable to residential radon, solid fuels, and particulate matter pollution under different sociodemographic transitions from 1990 to 2030. *Chest* **165**, 446–460 (2024).
- Stevic, R. & Milenkovic, B. Tracheobronchial tumors. *J. Thorac. Dis.* **8**, 3401–3413 (2016).
- Licht, P. B., Friis, S. & Pettersson, G. Tracheal cancer in Denmark: a nationwide study. *Eur. J. Cardio-Thorac. Surg.* **19**, 339–345 (2001).
- Coffin, C. M., Watterson, J., Priest, J. R. & Dehner, L. P. Extrapulmonary inflammatory myofibroblastic tumor (inflammatory pseudotumor). A clinicopathologic and immunohistochemical study of 84 cases. *Am. J. Surg. Pathol.* **19**, 859–872 (1995).
- Agrawal, S. et al. Survival trends in patients with tracheal carcinoma from 1973 to 2011. *Am. J. Otolaryngol.* **38**, 673–677 (2017).
- Lawrence, D. A., Branson, B., Oliva, I. & Rubinowitz, A. The wonderful world of the windpipe: a review of central airway anatomy and pathology. *Can. Assoc. Radiol. J.* **66**, 30–43 (2015).
- Zhengjiaiang, L., Pingzhang, T., Dechao, Z., Reddy-Kolanu, G. & Ilankovan, V. Primary tracheal tumours: 21 years of experience at Peking Union Medical College, Beijing, China. *J. Laryngol. Otol.* **122**, 1235–1240 (2008).
- Sherani, K., Vakil, A., Dodhia, C. & Fein, A. Malignant tracheal tumors: a review of current diagnostic and management strategies. *Curr. Opin. Pulm. Med.* **21**, 322–326 (2015).
- Macchiarini, P. Primary tracheal tumours. *Lancet Oncol.* **7**, 83–91 (2006).
- O'Donnell, J. S., Teng, M. W. L. & Smyth, M. J. Cancer immunoeediting and resistance to T cell-based immunotherapy. *Nat. Rev. Clin. Oncol.* **16**, 151–167 (2019).
- Oliveira, G. & Wu, C. J. Dynamics and specificities of T cells in cancer immunotherapy. *Nat. Rev. Cancer* **23**, 295–316 (2023).
- Gavrielatou, N., Doumas, S., Economopoulou, P., Foukas, P. G. & Psyri, A. Biomarkers for immunotherapy response in head and neck cancer. *Cancer Treat. Rev.* **84**, 101977 (2020).
- Tang, X. Y. et al. IGSF11 and VISTA: a pair of promising immune checkpoints in tumor immunotherapy. *Biomark. Res.* **10**, 49 (2022).
- Galon, J. & Bruni, D. Approaches to treat immune hot, altered and cold tumours with combination immunotherapies. *Nat. Rev. Drug Discov.* **18**, 197–218 (2019).
- Sebestyen, Z., Prinz, I., Déchanet-Merville, J., Silva-Santos, B. & Kuball, J. Translating gammadelta ($\gamma\delta$) T cells and their receptors into cancer cell therapies. *Nat. Rev. Drug Discov.* **19**, 169–184 (2020).
- Maller, B., Kaszuba, F. & Tanvetyanon, T. Complete tumor response of tracheal squamous cell carcinoma after treatment with pembrolizumab. *Ann. Thorac. Surg.* **107**, e273–e274 (2019).
- Tapias, L. F. et al. Programmed death ligand 1 and CD8+ immune cell infiltrates in resected primary tracheal malignant neoplasms. *Eur. J. Cardio-Thorac. Surg.* **55**, 691–698 (2019).
- Zheng, K. F. et al. PD-L1 expression and immune cells infiltration in primary tracheobronchial neoplasm. *Transl. Lung Cancer Res.* **10**, 4617–4630 (2021).
- Osho, A. A. et al. Successful treatment of an aggressive tracheal malignancy with immunotherapy. *Ann. Thorac. Surg.* **103**, e123–e125 (2017).
- Plasschaert, L. W. et al. A single-cell atlas of the airway epithelium reveals the CFTR-rich pulmonary ionocyte. *Nature* **560**, 377–381 (2018).
- Gao, R. et al. Delineating copy number and clonal substructure in human tumors from single-cell transcriptomes. *Nat. Biotechnol.* **39**, 599–608 (2021).
- Gulati, G. S. et al. Single-cell transcriptional diversity is a hallmark of developmental potential. *Science* **367**, 405–411 (2020).
- Madisson, E. et al. A spatially resolved atlas of the human lung characterizes a gland-associated immune niche. *Nat. Genet.* **55**, 66–77 (2023).
- La Manno, G. et al. RNA velocity of single cells. *Nature* **560**, 494–498 (2018).
- Saw, P. E., Liu, Q., Wong, P. P. & Song, E. Cancer stem cell mimicry for immune evasion and therapeutic resistance. *Cell Stem Cell* <https://doi.org/10.1016/j.stem.2024.06.003> (2024).

27. Wang, Y. et al. Centrosome-associated regulators of the G2/M checkpoint as targets for cancer therapy. *Mol. Cancer* **8**, 8 (2009).
28. Yao, Y. et al. CDK7 controls E2F- and MYC-driven proliferative and metabolic vulnerabilities in multiple myeloma. *Blood* **141**, 2841–2852 (2023).
29. Orlikova-Boyer, B. et al. Antileukemic potential of methylated indolequinone MAC681 through immunogenic necroptosis and PARP1 degradation. *Biomark. Res.* **12**, 47 (2024).
30. Röhrig, F. & Schulze, A. The multifaceted roles of fatty acid synthesis in cancer. *Nat. Rev. Cancer* **16**, 732–749, <https://doi.org/10.1038/nrc.2016.89> (2016).
31. Takebe, N. et al. Targeting Notch, Hedgehog, and Wnt pathways in cancer stem cells: clinical update. *Nat. Rev. Clin. Oncol.* **12**, 445–464 (2015).
32. Musa, J., Aynaud, M. M., Mirabeau, O., Delattre, O. & Grünewald, T. G. MYBL2 (B-Myb): a central regulator of cell proliferation, cell survival and differentiation involved in tumorigenesis. *Cell Death Dis.* **8**, e2895 (2017).
33. Yuan, Z. et al. Extracellular matrix remodeling in tumor progression and immune escape: from mechanisms to treatments. *Mol. Cancer* **22**, 48 (2023).
34. Li, X. et al. Single-cell RNA sequencing reveals a pro-invasive cancer-associated fibroblast subgroup associated with poor clinical outcomes in patients with gastric cancer. *Theranostics* **12**, 620–638 (2022).
35. Liberzon, A. et al. The Molecular Signatures Database (MSigDB) hallmark gene set collection. *Cell Syst.* **1**, 417–425 (2015).
36. Yang, X. et al. FAP promotes immunosuppression by cancer-associated fibroblasts in the tumor microenvironment via STAT3-CCL2 signaling. *Cancer Res.* **76**, 4124–4135 (2016).
37. Cords, L. et al. Cancer-associated fibroblast classification in single-cell and spatial proteomics data. *Nat. Commun.* **14**, 4294 (2023).
38. Elyada, E. et al. Cross-species single-cell analysis of pancreatic ductal adenocarcinoma reveals antigen-presenting cancer-associated fibroblasts. *Cancer Discov.* **9**, 1102–1123 (2019).
39. Baudino, T. A. et al. c-Myc is essential for vasculogenesis and angiogenesis during development and tumor progression. *Genes Dev.* **16**, 2530–2543 (2002).
40. Baumgart, A. et al. Opposing role of Notch1 and Notch2 in a Kras(G12D)-driven murine non-small cell lung cancer model. *Oncogene* **34**, 578–588 (2015).
41. Bagati, A. et al. Integrin α v β 6-TGF β -SOX4 pathway drives immune evasion in triple-negative breast cancer. *Cancer Cell* **39**, 54–67.e59 (2021).
42. Blatti, C. et al. Bayesian machine learning enables identification of transcriptional network disruptions associated with drug-resistant prostate cancer. *Cancer Res.* **83**, 1361–1380 (2023).
43. Reith, W. & Mach, B. The bare lymphocyte syndrome and the regulation of MHC expression. *Annu. Rev. Immunol.* **19**, 331–373 (2001).
44. Hu, Z. et al. The transcription factor RFX5 coordinates antigen-presenting function and resistance to nutrient stress in synovial macrophages. *Nat. Metab.* **4**, 759–774 (2022).
45. Chu, Y. et al. Pan-cancer T cell atlas links a cellular stress response state to immunotherapy resistance. *Nat. Med.* **29**, 1550–1562 (2023).
46. Yang, S. et al. Machine learning-based integration develops a stress response stated T cell (Tstr)-related score for predicting outcomes in clear cell renal cell carcinoma. *Int. Immunopharmacol.* **132**, 112017 (2024).
47. Zhang, Y. et al. Close the cancer-immunity cycle by integrating lipid nanoparticle-mRNA formulations and dendritic cell therapy. *Nat. Nanotechnol.* **18**, 1364–1374 (2023).
48. Yu, W., Wang, Y. & Guo, P. Notch signaling pathway dampens tumor-infiltrating CD8(+) T cells activity in patients with colorectal carcinoma. *Biomed. Pharmacother.* **97**, 535–542 (2018).
49. Li, S., Wang, Z. & Li, X. J. Notch signaling pathway suppresses CD8(+) T cells activity in patients with lung adenocarcinoma. *Int. Immunopharmacol.* **63**, 129–136 (2018).
50. Takeuchi, Y. et al. Highly immunogenic cancer cells require activation of the WNT pathway for immunological escape. *Sci. Immunol.* **6**, eabc6424 (2021).
51. Jindal, A., Bal, A. & Agarwal, R. Inflammatory myofibroblastic tumor of the trachea in the pediatric age group: case report and systematic review of the literature. *J. Bronchol. Interv. Pulmonol.* **22**, 58–65 (2015).
52. Maffia, P., Mauro, C., Case, A. & Kemper, C. Canonical and non-canonical roles of complement in atherosclerosis. *Nat. Rev. Cardiol.* <https://doi.org/10.1038/s41569-024-01016-y> (2024).
53. Lin, L. R. et al. Akt, mTOR and NF- κ B pathway activation in *Treponema pallidum* stimulates M1 macrophages. *Int. Immunopharmacol.* **59**, 181–186 (2018).
54. Wang, Y. C. et al. Notch signaling determines the M1 versus M2 polarization of macrophages in antitumor immune responses. *Cancer Res.* **70**, 4840–4849 (2010).
55. Chen, D. et al. Chloroquine modulates antitumor immune response by resetting tumor-associated macrophages toward M1 phenotype. *Nat. Commun.* **9**, 873 (2018).
56. Ruffell, B. & Coussens, L. M. Macrophages and therapeutic resistance in cancer. *Cancer Cell* **27**, 462–472 (2015).
57. Efremova, M., Vento-Tormo, M., Teichmann, S. A. & Vento-Tormo, R. CellPhoneDB: inferring cell-cell communication from combined expression of multi-subunit ligand-receptor complexes. *Nat. Protoc.* **15**, 1484–1506 (2020).
58. Wang, K. et al. Di-methylation of CD147-K234 promotes the progression of NSCLC by enhancing lactate export. *Cell Metab.* **33**, 160–173.e166 (2021).
59. Cui, H. Y. et al. CD147 receptor is essential for TFF3-mediated signaling regulating colorectal cancer progression. *Signal Transduct. Target. Ther.* **6**, 268 (2021).
60. Chen, Y. et al. CD147 regulates antitumor CD8(+) T-cell responses to facilitate tumor-immune escape. *Cell. Mol. Immunol.* **18**, 1995–2009 (2021).
61. Yurchenko, V., Constant, S., Eisenmesser, E. & Bukrinsky, M. Cyclophilin-CD147 interactions: a new target for anti-inflammatory therapeutics. *Clin. Exp. Immunol.* **160**, 305–317 (2010).
62. Han, J. M., Sohng, J. K., Lee, W. H., Oh, T. J. & Jung, H. J. Identification of cyclophilin A as a potential anticancer target of novel narginecin A1 analog in AGS gastric cancer cells. *Int. J. Mol. Sci.* **22**, <https://doi.org/10.3390/ijms22052473> (2021).
63. Ho, P. et al. The CD58-CD2 axis is co-regulated with PD-L1 via CMTM6 and shapes anti-tumor immunity. *Cancer Cell* **41**, 1207–1221.e1212 (2023).
64. Pitt, J. M. et al. Targeting the tumor microenvironment: removing obstruction to anticancer immune responses and immunotherapy. *Ann. Oncol.* **27**, 1482–1492 (2016).
65. Wang, Y. et al. Circadian regulation of cancer stem cells and the tumor microenvironment during metastasis. *Nat. Cancer* **5**, 546–556 (2024).
66. Veneziani, A. C. et al. Heterogeneity and treatment landscape of ovarian carcinoma. *Nat. Rev. Clin. Oncol.* **20**, 820–842 (2023).
67. Mempel, T. R., Lill, J. K. & Altenburger, L. M. How chemokines organize the tumour microenvironment. *Nat. Rev. Cancer* **24**, 28–50 (2024).
68. de Jong, M. M. E. et al. An IL-1 β -driven neutrophil-stromal cell axis fosters a BAFF-rich protumor microenvironment in individuals with multiple myeloma. *Nat. Immunol.* **25**, 820–833 (2024).
69. Rerkpichaisuth, V. & Hung, Y. P. Mesenchymal tumours of the pleura: review and update. *Histopathology* **84**, 163–182 (2024).
70. Goveia, J. et al. An integrated gene expression landscape profiling approach to identify lung tumor endothelial cell heterogeneity and angiogenic candidates. *Cancer Cell* **37**, 21–36.e13 (2020).

71. Shu, C. et al. Diagnosis and treatment of primary tracheobronchial tumors. *Cancer Med.* **14**, e70893 (2025).
72. Yang, C. J. et al. Impact of positive margins and radiation after tracheal adenoid cystic carcinoma resection on survival. *Ann. Thorac. Surg.* **109**, 1026–1032 (2020).
73. Wang, Y. et al. Tracheobronchial adenoid cystic carcinoma: 50-year experience at the National Cancer Center, China. *Ann. Thorac. Surg.* **108**, 873–882 (2019).
74. Jia, Y., Liu, Y., Yang, H. & Yao, F. Adenoid cystic carcinoma: insights from molecular characterization and therapeutic advances. *MedComm* **5**, e734 (2024).

Acknowledgements

This work was supported by Shaanxi Outstanding Youth Natural Science Foundation (2024-JC-JCQN-79); Shaanxi Provincial Health and Wellness Chest Tumor Basic Research and Translational Surgery Precision Diagnosis and Treatment Scientific Research Innovation Team (No. 2025TD-04); the National Natural Science Foundation of China (82070101); Young Scientific and Technological Talent Autonomous Program (2024). The authors would like to appreciate Editage for English language editing and biorender for picture drawing (<https://app.biorender.com/>).

Author contributions

Z.J.B., M.N., and Y.X.L. determined the project and assisted in the revision of the manuscript. S.C., T.X.Y., Z.K.F., and Z.R.Z. wrote the manuscript. All authors participated in data collection and interpretation. All authors read and approved the final manuscript.

Competing interests

The authors declares no competing interests.

Additional information

Supplementary information The online version contains supplementary material available at <https://doi.org/10.1038/s41698-025-01203-1>.

Correspondence and requests for materials should be addressed to Xiaolong Yan, Nan Ma or Jinbo Zhao.

Reprints and permissions information is available at <http://www.nature.com/reprints>

Publisher's note Springer Nature remains neutral with regard to jurisdictional claims in published maps and institutional affiliations.

Open Access This article is licensed under a Creative Commons Attribution-NonCommercial-NoDerivatives 4.0 International License, which permits any non-commercial use, sharing, distribution and reproduction in any medium or format, as long as you give appropriate credit to the original author(s) and the source, provide a link to the Creative Commons licence, and indicate if you modified the licensed material. You do not have permission under this licence to share adapted material derived from this article or parts of it. The images or other third party material in this article are included in the article's Creative Commons licence, unless indicated otherwise in a credit line to the material. If material is not included in the article's Creative Commons licence and your intended use is not permitted by statutory regulation or exceeds the permitted use, you will need to obtain permission directly from the copyright holder. To view a copy of this licence, visit <http://creativecommons.org/licenses/by-nc-nd/4.0/>.

© The Author(s) 2025